# Wolter Optics for Neutron Transport

Summer internship at the Institut Laue-Langevin under the supervision of Dr Richard Wagner

Niya Petkova

May - August 2022

# Contents

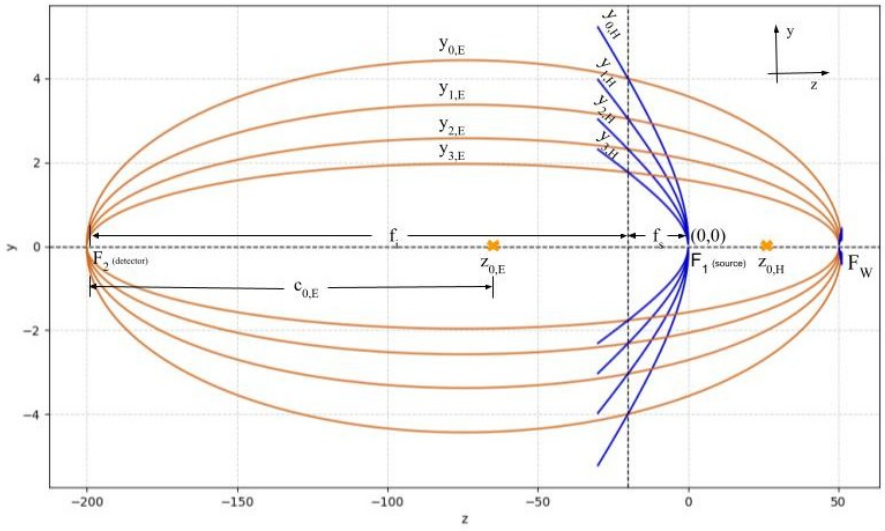


Figure 1: Nested Wolter Optics

# 1 Preliminaries

This document outlines a method for defining a system of nested Wolter optics layers as depicted on Figure 1. A Wolter system consists of an ellipse/a parabola and a hyperbola that have one coinciding focus ($F_w$). There are three possible ways to construct a focusing device like this, the so called Wolter optics of Type I, II and III [1]. Such optical designs have proven useful for the construction of X-ray telescopes and microscopes [1], [2], [3], but this document will focus on their possible implementation in the field of neutron transport, and specifically for the NNBAR experiment of the HighNESS project. The proposed optics will be of Type I, so that it can provide focusing of a close object to a detector that is further away, functioning like a larger scale microscope [1] [4].

To understand the methodology that follows, it is important to first get acquainted with the geometric layout assumed by the document. The origin of the coordinate system is taken to be the position of the neutron source, which is sitting at the unshared focal point of the outermost hyperbola ($F_1$ on Figure 1). The neutron detector is placed at the remaining focal point of the outermost ellipse ($F_2$ on Figure 1). The semi-major axes of the ellipses stretch in the z-direction of the coordinate system to comply with the notation of the neutron ray-tracing program McStas. The semi-minor axes extend into the y-direction. The x-axis goes along the width of the mirrors, which is restricted externally by the parameters of the neutron facility.

The condition that the intersection point of the hyperbolas and the ellipses remains at the same z-coordinate for all nested layers is artificially imposed. Hence, three parameters stay constant for all mirrors in the system: the distances $f_s$ and $f_i$ which define the z-position of the hyperbola-ellipse intersection points, and the horizontal length of hyperbolas, $L_H$, which is taken to be the same for all hyperbolic mirrors.

For the parameters that change in between layers, a subscript is supplied to each nested level. For a system of n levels, the subscripts range from 0 to (n-1). The mirrors are numbered from the outermost layer (index 0) going inwards to levels with larger indices. If a general parameter derivation is discussed, the index $n$ is used to indicate universality of the equations. If the derivation is only applicable to a specific level, then the index of that level is supplied.

Here is a list of all used parameters:

- $R_n$ - intersection point of the ellipse and the hyperbola of the nth nested level
- $r_n$ - height of the nth layer of optics at $R_n$ ($r_0$ given by the set-up of the experiment - maximum allowed height of the optics)
- $f_s$ - z-distance from the source to $R_n$ (constant for all layers)
- $f_i$ - z-distance from $R_n$ to the detector (constant for all layers)
- $f = f_i + f_s$ - z-distance between the source and the detector (constant for all layers)
- $L_H$ - z-length of a hyperbolic section of the optics (constant for all layers, $L_H \leq f_s$)
- $L_{n,E}$ - z-length of an ellipsoid section of the optics (approx. constant for all layers, $L_{n,E} \leq f_i$)
- $L_n$(or $L_{optic}$) $= L_H + L_E$ - z-length of the nth Wolter layer
- $b_{n,E}$ and $b_{n,H}$ - semi-minor axes of the nth ellipse and hyperbola
- $a_{n,E}$ and $a_{n,H}$ - semi-major axes of the nth ellipse and hyperbola
- $c_{n,E}$ and $c_{n,H}$ - focal distances of the nth ellipse and hyperbola
- $y_{n,E}$ and $y_{n,H}$ - equations of the nth ellipse and hyperbola
- $\beta_1$ - angle between the optical axis and the ray passing from the source to $R_0$
- $\beta_2$ - angle between the optical axis and the ray passing from $R_0$ to the detector

- m - reflectivity of the mirrors (m = 6 is assumed for all simulated mirrors)

Sections 3 and 4 of this document provide a general background for the creation of nested arrays of Wolter optics, while the rest focuses on McStas and the simulations performed for the NNBAR experiment. The supplied results employ the specific parameters for the NNBAR experiment, but the code itself is not limited to NNBAR. A more direct introduction to the code is provided in Appendix III.

# 2 On the NNBAR

The NNBAR is an experiment proposed by the HighNESS project at the ESS. Its purpose is to search for a neutron-antineutron oscillation, which could provide an explanation to the matter-antimatter asymmetry observed in the universe [5], [6]. Such an experiment was previously performed at the ILL without being able to discover the desired oscillation [7]. The aim of the NNBAR is to improve upon this first experiment by at least three orders of magnitude [5], [8]. Hence, the unit figure of merit (FOM) is introduced, and a FOM of 1 corresponds to the efficiency of the original ILL trial. An improvement of three orders of magnitude would imply a FOM of 1000. Since the NNBAR will be running for 3 years, this value can be reduced to $1000/3 \approx 333$ per year. All significant results of FOM $> 300$ are highlighted in the document.

The FOM value is based on the probability of finding a neutron-antineutron oscillation, and there are two main parameters that influence this probability, the number of neutrons reaching the detector (N) and the time of flight (t) [5]. The second has a bigger weighting, as the FOM scales with the square of the time of flight, where t of a neutron is defined as the time it takes for the particle to reach the detector after its last interaction with the reflector. The set-up of the experiment is very simple; it only consists of a source from which neutrons are guided away via a large beam port opening (LBP), followed by an optical system like the proposed one, or by a guide, to a detector positioned at 200 m away from the source [5]. Since the aim of the optics would be to maximize the FOM, it will have to provide an optimal $Nt^2$ by guiding as many neutrons as possible without reducing their time of flight.

A conventional neutron guide might not be the best option, as it would transport many of the neutrons via multiple reflections, thus significantly reducing their time of flight, and absorbing more of the original flux. Thus, it is sensible to look for an optical system that could be placed closer to the source to maximize the time of flight, while focusing the neutrons, so that more of them are accepted by the detector. To construct such a system, a method for building a single-layer Wolter system is first discussed in the following section.

# 3 Top Layer of the System

First, we consider only the outer ellipse and hyperbola (layer 0 on Figure 1), and describe a method for obtaining their equations from the given parameters ($f_s$, $f_i$ and $r_0$). Most of these equations for single-layer Wolter optics have already been introduced by Khaykovich et al [9], but are derived in greater detail here.

## 3.1 Ellipse

There are two general equations governing the behavior of an ellipse:

$$\frac{(z-h_E)^2}{a_E^2}+\frac{(y_E-k_E)^2}{b_E^2}=1 \tag{1}$$

and

$$a_E^2=c_E^2+b_E^2 \tag{2}$$

where $(h_E, k_E)$ is the position of the center of the ellipse, and z is the coordinate at which $y_E$ is evaluated.

We use these equations to describe an ellipse $y_{0,E}$ centered at $(z_{0,E}, 0)$, as on Figure 1. Its equation is

$$\frac{(z-z_{0,E})^2}{a_{0,E}^2}+\frac{y_{0,E}^2}{b_{0,E}^2}=1 \tag{3}$$

But we can substitute $z_{0,E}=-(c_{0,E}-2c_{0,H})$:

$$\frac{(z+c_{0,E}-2c_{0,H})^2}{a_{0,E}^2}+\frac{y_{0,E}^2}{b_{0,E}^2}=1 \tag{4}$$

We evaluate this equation at the intersection point of the two mirrors, $z=-f_s$, where $y_{0,E}(-f_s)=r_0$:

$$\frac{(-f_s+c_{0,E}-2c_{0,H})^2}{a_{0,E}^2}+\frac{r_0^2}{b_{0,E}^2}=1 \tag{5}$$

Rearranging, we get

$$\frac{r_0^2}{b_{0,E}^2}=1-\frac{(-f_s+c_{0,E}-2c_{0,H})^2}{a_{0,E}^2} \tag{6}$$

Hence, the two equations describing an ellipse in the coordinate system of Figure 1 are:

$$b_{0,E}^2=\frac{r_0^2a_{0,E}^2}{(a_{0,E}^2-(-f_s+c_{0,E}-2c_{0,H})^2)} \tag{7}$$

and

$$a_{0,E}^2 = c_{0,E}^2 + b_{0,E}^2 \tag{8}$$

where we can notice that if $c_{0,E}$ and $c_{0,H}$ are known, the system of equations will be solvable.

## 3.2 Hyperbola

The two equations defining a hyperbola that opens to the left and right and is centered at $(h_H, k_H)$ are:

$$\frac{(z - h_H)^2}{a_H^2} - \frac{(y_H - k_H)^2}{b_H^2} = 1 \tag{9}$$

and

$$c_H^2 = a_H^2 + b_H^2 \tag{10}$$

The outer hyperbola on Figure 1 is centered at $(z_{0,H}, 0)$ and has the equation

$$\frac{(z - z_{0,H})^2}{a_{0,H}^2} - \frac{y_{0,H}^2}{b_{0,H}^2} = 1 \tag{11}$$

But $z_{0,H} = c_{0,H}$, so

$$\frac{(z - c_{0,H})^2}{a_{0,H}^2} - \frac{y_{0,H}^2}{b_{0,H}^2} = 1 \tag{12}$$

Evaluating at the intersection point ($z = -f_s$, $y_{0,H}(-f_s) = r_0$), we get:

$$\frac{(-f_s - c_{0,H})^2}{a_{0,H}^2} - \frac{r_0^2}{b_{0,H}^2} = 1 \tag{13}$$

Rearranging:

$$\frac{r_0^2}{b_{0,H}^2} = \frac{(-f_s - c_{0,H})^2}{a_{0,H}^2} - 1 \tag{14}$$

Hence, the two equations defining the top hyperbola on Figure 1 are:

$$b_{0,H}^2 = \frac{r_0^2 a_{0,H}^2}{(f_s + c_{0,H})^2 - a_{0,H}^2} \tag{15}$$

and

$$a_{0,H}^2 = c_{0,H}^2 - b_{0,H}^2 \tag{16}$$

where, again, this system of equations will be solvable once $c_{0,H}$ is defined.

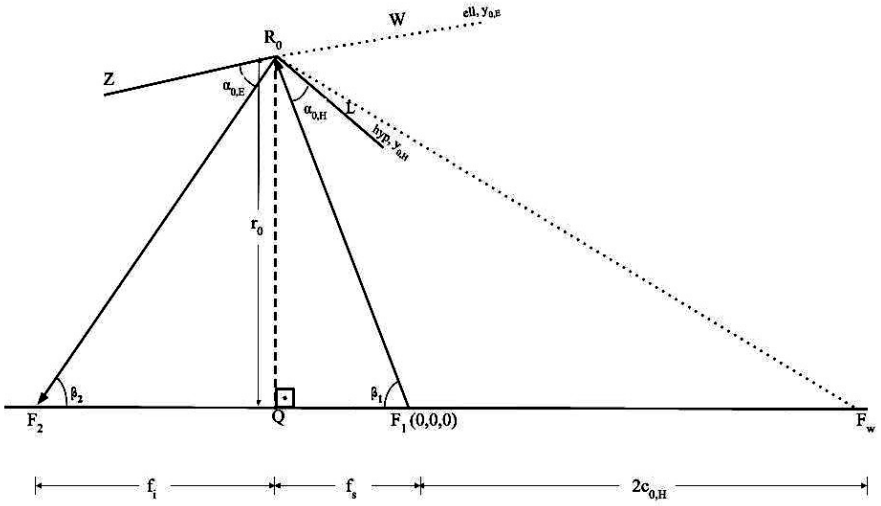


Figure 2: Single Layer Wolter System (figure not to scale)

## 3.3 Focal distances of the top ellipse and hyperbola

Equations 7-8 and 15-16 suggest that if one of the parameters of each mirror is known ($a_{0,E}, b_{0,E}$ or $c_{0,E}$ for the ellipse, $a_{0,H}, b_{0,H}$ or $c_{0,H}$ for hyperbola), there will be as many equations as unknowns, so we will be able to define the system. Hence, we try to find the focal distances $c_{0,E}$ and $c_{0,H}$, but to do so we need expressions for some of the angles in the system.

### 3.3.1 Grazing Angles at Point $R_n$

Let us call the angles of incidence and reflection from the two mirrors at the point $R_0$ $\alpha_{0,E}$ and $\alpha_{0,H}$ as on Figure 2. We will now convince ourselves that the angles $\angle LR_0F_w$ and $\angle F_wR_0W$ are also equal to $\alpha_{0,H}$ and $\alpha_{0,E}$, respectively.

As conic sections, hyperbolas inherit the peculiar property that the reflection of a ray incoming from one of their foci appears to be originating from the other focus (proof in Appendix I). Hence, the reflected ray $\overrightarrow{R_0K}$ lies on ray $\overrightarrow{F_wK}$ on Figure 3 and $\angle KR_0F_w$ is a straight angle:

$$2(90^\circ - \alpha_{0,H}) + \alpha_{0,H} + \angle LR_0F_w = 180^\circ \tag{17}$$

$$180^\circ - \alpha_{0,H} + \angle LR_0F_w = 180^\circ \tag{18}$$

And so

$$\angle LR_0F_w = \alpha_{0,H} \tag{19}$$

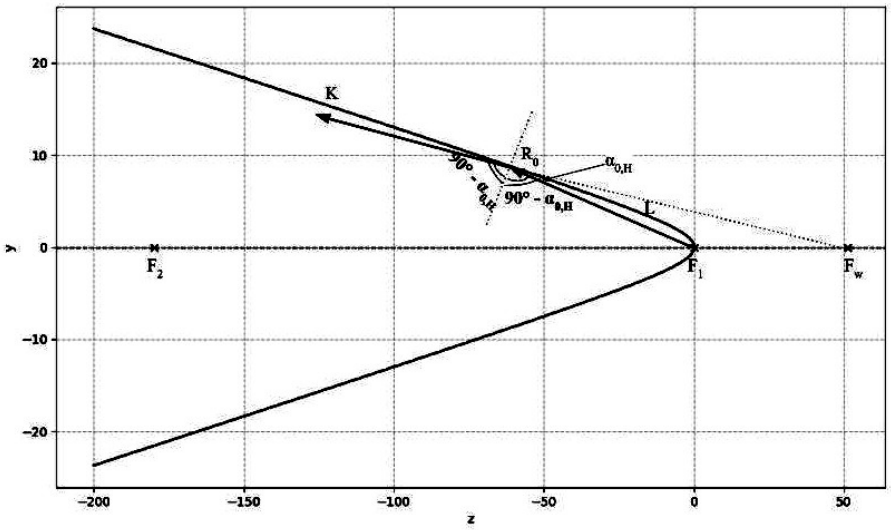


Figure 3: Reflection by a Hyperbola

As another conic section, an ellipse is defined as the locus of points for which the sum of distances to each of the foci is preserved. To satisfy this condition, a ray passing through one of the foci and incident on any point on the surface of the ellipse has to reflect back to the other focus (proof in Appendix 1). Hence, ray $\overrightarrow{R_0F_2}$ on Figure 4 must be a reflection of ray $\overrightarrow{F_wR_0}$.

Thus, by the law of reflection:

$$\angle F_2R_0Z = \angle F_wR_0W = \alpha_{0,E} \tag{20}$$

So angles $\angle LR_0F_w$ and $\angle F_wR_0W$ on Figure 2 are indeed the same as the

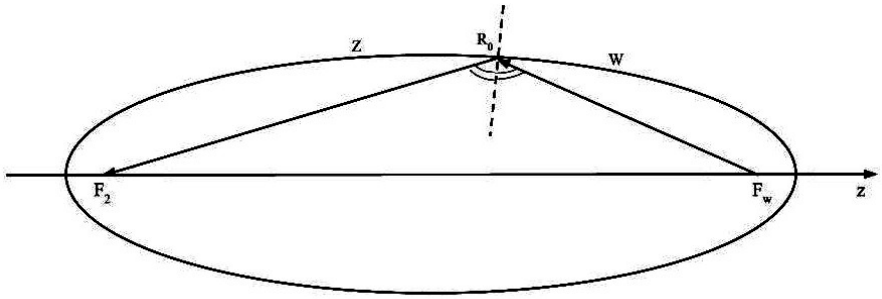


Figure 4: Reflection by an Ellipse

angles of reflection from the hyperbola and the ellipse, respectively. We now use this fact to test one peculiar angle property of Wolter optics.

From triangle $F_1R_0F_w$ on Figure 2 we have

$$(180^\circ - \beta_1) + 2\alpha_{0,H} + \angle F_1F_wR_0 = 180^\circ \tag{21}$$

$$\angle F_1F_wR_0 = \beta_1 - 2\alpha_{0,H} \tag{22}$$

Taking the tan of this angle in triangle $QR_0F_w$, we get

$$tan(\beta_1 - 2\alpha_{0,H}) = \frac{r_0}{f_s + 2c_{0,H}} \tag{23}$$

From this we derive an expression for the angle $\alpha_{0,H}$:

$$\alpha_{0,H} = \frac{\beta_1 - arctan(\frac{r_0}{f_s+2c_{0,H}})}{2} \tag{24}$$

From the external angles to the triangle $F_2R_0F_1$, we also have that

$$\beta_1 + \beta_2 = 2(\alpha_{0,E} + \alpha_{0,H}) \tag{25}$$

$$\alpha_{0,E} = \frac{\beta_1 + \beta_2}{2} - \alpha_{0,H} \tag{26}$$

The angles $\beta_1$ and $\beta_2$ can be found from the dimensions of triangles $QR_0F_1$ and $QR_0F_2$:

$$tan(\beta_1) = \frac{r_0}{f_s} \rightarrow \beta_1 = \arctan(\frac{r_0}{f_s}) \tag{27}$$

$$tan(\beta_2) = \frac{r_0}{f_i} \rightarrow \beta_2 = \arctan(\frac{r_0}{f_i}) \tag{28}$$

We substitute these expressions into equations 24 and 26 to get

$$\alpha_{0,H} = \frac{\arctan(\frac{r_0}{f_s}) - \arctan(\frac{r_0}{f_s+2c_{0,H}})}{2} \tag{29}$$

and

$$\alpha_{0,E} = \frac{\arctan(\frac{r_0}{f_s}) + \arctan(\frac{r_0}{f_i})}{2} - \alpha_{0,H} \tag{30}$$

For the particular application of neutron transport, these angles must be very small, as neutron reflections occur only at tiny glancing angles (for nickel and m = 1, $\theta_{critical} = 0.0173\lambda$ rad) [10]. To maximize the number of neutrons that are transported by the system, Khaykovich et al and Bagdasarova [9], [11] assume that the glancing angles at both surfaces are equal. This condition is tested by plotting the angles $\alpha_{0,H}$ and $\alpha_{0,E}$ for a range of different values of

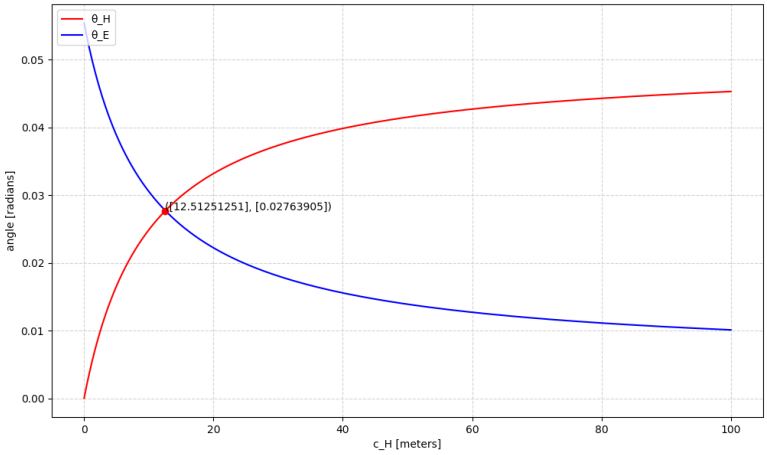


Figure 5: Grazing angles at intersection point against different values of $c_H$

$c_{0,H}$ on Figure 5. For the other parameters of the system, the dimensions of the NNBAR experiment are used: $r_0 = 2$ m, $f_i = 180$ m, $f_s = 20$ m.

As we can see on the plot, the angles differ significantly for most focal distances of the hyperbola, so the condition that they are equal is not inherent in a Wolter system. It is possible that Wolter arrangements where one of the mirrors accepts more neutrons than the other turn out to have some advantages over the symmetric ones, but they will not be the focus of this narrative. Instead, the following section will aim to derive formulas for $c_{0,H}$ that return the value of 12.5 m, characteristic of the symmetric NNBAR system on Figure 5.

Assuming that the two glancing angles are equal, and calling them both $\theta_0$ ($\alpha_{0,E} = \alpha_{0,H} = \theta_0$), their value can be derived from equation 26:

$$\theta_0 = \frac{\beta_1 + \beta_2}{4} = \frac{1}{4}(\arctan(\frac{r_0}{f_i}) + \arctan(\frac{r_0}{f_s})) \tag{31}$$

### 3.3.2 Focal distances $c_{0,E}$ and $c_{0,H}$

Equation 23 and the assumption of equal glancing angles are now used to derive expressions for the focal distances of the top ellipse and hyperbola:

$$\tan(\beta_1 - 2\alpha_{0,H}) = \frac{r_0}{f_s + 2c_{0,H}} \tag{32}$$

$$r_0 = \tan(\beta_1 - 2\theta_0)(f_s + 2c_{0,H}) \tag{33}$$

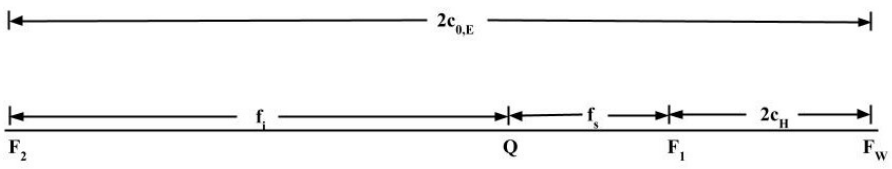


Figure 6: Parameters of Wolter System

$$2c_{0,H} + f_s = \frac{r_0}{\tan(\beta_1 - 2\theta_0)} \tag{34}$$

$$c_{0,H} = \frac{1}{2}\left[\frac{r_0}{\tan(\beta_1 - 2\theta_0)} - f_s\right] \tag{35}$$

where $\theta_0$ is given by equation 31. When the NNBAR parameters are plugged into this expression, it produces exactly the value given by the equal angles assumption on Figure 5.

An expression for the focal distance of the ellipse is also defined by relating $c_{0,E}$ to the values of $f_s, f_i$ and $c_{0,H}$ as on Figure 6:

$$2c_{0,E} = f_i + f_s + 2c_{0,H} \tag{36}$$

$$c_{0,E} = c_{0,H} + \frac{f_s + f_i}{2} \tag{37}$$

### 3.4 Solving for the parameters of the top ellipse

We use the above equations to define a general expression for each of the parameters of the ellipse ($a_{0,E}, b_{0,E}$ and $c_{0,E}$) from the givens ($f_i, f_s, r_0$).

From equation 7, we have

$$b_{0,E}^2 = \frac{r_0^2 a_{0,E}^2}{(a_{0,E}^2 - L^2)} \tag{38}$$

where $L = -f_s + c_{0,E} - 2c_{0,H}$.

Substituting $b_{0,E}^2 = a_{0,E}^2 - c_{0,E}^2$ from equation 8:

$$a_{0,E}^2 - c_{0,E}^2 = \frac{r_0^2 a_{0,E}^2}{a_{0,E}^2 - L^2} \tag{39}$$

$$\frac{r_0^2 a_{0,E}^2}{a_{0,E}^2 - L^2} - a_{0,E}^2 + c_{0,E}^2 = 0 \tag{40}$$

Noting the condition that $a_{0,E}^2 \neq L$, we have:

$$r_0^2 a_{0,E}^2 + (-a_{0,E}^2 + c_{0,E}^2)(a_{0,E}^2 - L^2) = 0 \tag{41}$$

This simplifies to the quadratic equation:

$$a_{0,E}^4 - a_{0,E}^2(L^2 + c_{0,E}^2 + r_0^2) + c_{0,E}^2 L^2 = 0 \tag{42}$$

which has roots

$$a_{0,E}^2 = \frac{(L^2 + c_{0,E}^2 + r_0^2) \ \pm \ \sqrt{(L^2 + c_{0,E}^2 + r_0^2)^2 - 4c_{0,E}^2 L^2}}{2} \tag{43}$$

We take the higher value (otherwise later $b_E$ wouldn't be well-defined). Hence the ellipse has a major axis of length

$$a_{0,E} = \left[\frac{(L^2 + c_{0,E}^2 + r_0^2) \ + \ \sqrt{(L^2 + c_{0,E}^2 + r_0^2)^2 - 4c_{0,E}^2 L^2}}{2}\right]^{\frac{1}{2}} \tag{44}$$

where $L = (-f_s + c_{0,E} - 2c_{0,H})$ and $c_{0,E}$ is expressed from equations 35 and 37 as

$$c_{0,E} = \frac{f_s + f_i}{2} + \frac{1}{2}\left[\frac{r_0}{\tan(\beta_1 - 2\theta_0)} - f_s\right] \tag{45}$$

with $\theta_0$ given by equation 31 as

$$\theta_0 = \frac{1}{4}(arctan(\frac{r_0}{f_i}) + arctan(\frac{r_0}{f_s})) \tag{46}$$

Thus, equations 44 and 45 fully define $a_{0,E}$ and $c_{0,E}$, so we can use equation 8, $b_{0,E}^2 = a_{0,E}^2 - c_{0,E}^2$, to find $b_{0,E}$ and complete the mathematical description of the top ellipse.

### 3.5 Solving for the parameters of the top hyperbola

Similarly, we now define the parameters of the hyperbola ($a_{0,H}, b_{0,H}$ and $c_{0,H}$) in terms of the givens ($f_s, f_i, r_0$).

From equation 15, it follows:

$$b_{0,H}^2 = \frac{r_0^2 a_{0,H}^2}{(f_s + c_{0,H})^2 - a_{0,H}^2} \tag{47}$$

Substituting $b_{0,H}^2 = c_{0,H}^2 - a_{0,H}^2$ from equation 16:

$$c_{0,H}^2 - a_{0,H}^2 = \frac{r_0^2 a_{0,H}^2}{(f_s + c_{0,H})^2 - a_{0,H}^2} \tag{48}$$

Noting the condition that $a_{0,H}^2 \neq (f_s + c_{0,H})^2$, we have:

$$(c_{0,H}^2 - a_{0,H}^2)((f_s + c_{0,H})^2 - a_{0,H}^2) = r_0^2 a_{0,H}^2 \tag{49}$$

This simplifies to the quadratic equation:

$$a_{0,H}^4 - a_{0,H}^2 N + c_{0,H}^2 (f_s + c_{0,H})^2 = 0 \tag{50}$$

where

$$N = c_{0,H}^2 + (f_s + c_{0,H})^2 + r_0^2 \tag{51}$$

This has roots

$$a_{0,H}^2 = \frac{N \ \pm \ \sqrt{N^2 - 4c_{0,H}^2 (f_s + c_{0,H})^2}}{2} \tag{52}$$

We take the lower value (empirically tested with Khaykovich et al. data).

Hence the hyperbola has a major axis of length

$$a_{0,H} = \left[ \frac{N \ - \ \sqrt{N^2 - 4c_{0,H}^2 (f_s + c_{0,H})^2}}{2} \right]^{\frac{1}{2}} \tag{53}$$

where $N = c_{0,H}^2 + (f_s + c_{0,H})^2 + r_0^2$ and $c_{0,H}$ is defined by equations 31 and 35.

Thus, equation 53 fully defines $a_{0,H}$, so we can use equation 16 ($b_{0,H}^2 = c_{0,H}^2 - a_{0,H}^2$) to find $b_{0,H}$ and construct the top hyperbola.

# 4 Nesting Layers of Wolter Optics

Following similar considerations as in the previous section, the formulas there can be extended to any layer of the nested system. For the n-th hyperbola, equations 53 and 35 can be generalized to get

$$a_{n,H} = \left[ \frac{N \ - \ \sqrt{N^2 - 4c_{n,H}^2 (f_s + c_{n,H})^2}}{2} \right]^{\frac{1}{2}} \tag{54}$$

where $N = c_{n,H}^2 + (f_s + c_{n,H})^2 + r_n^2$ and $c_{n,H}$ is defined as

$$c_{n,H} = \frac{f_s \theta_n}{(\frac{r_n}{f_s} - 2\theta_n)} \tag{55}$$

with

$$\theta_n = \frac{1}{4}(arctan(\frac{r_n}{f_i}) + arctan(\frac{r_n}{f_s})) \tag{56}$$

Equation 12 can also be generalized to produce the height of any nested hyperbola at a given point z:

$$y_{n,H} = b_{n,H}\sqrt{\frac{(z - c_{n,H})^2}{a_{n,H}^2} - 1} \tag{57}$$

The semi-minor axis is given by equation 16: $b_{n,H}^2 = c_{n,H}^2 - a_{n,H}^2$.

For the n-th ellipse, we would have the following generalizations of equations 44 through 46:

$$a_{n,E} = \left[\frac{(L^2 + c_{n,E}^2 + r_n^2) \ + \ \sqrt{(L^2 + c_{n,E}^2 + r_n^2)^2 - 4c_{n,E}^2 L^2}}{2}\right]^{\frac{1}{2}} \tag{58}$$

where $L = (-f_s + c_{n,E} - 2c_{n,H})$ and

$$c_{n,E} = c_{n,H} + \frac{f_s + f_i}{2} \tag{59}$$

Equation 4 can also be transformed so that it can be used to calculate the ellipse height at a given point along the z-axis:

$$y_{n,E}(z) = b_{n,E}\sqrt{1 - \frac{(z + c_{n,E} - 2c_{n,H})^2}{a_{n,E}^2}} \tag{60}$$

where $b_{n,E}^2 = a_{n,E}^2 - c_{n,E}^2$.

We can notice that in these equations the only unknown is the height $r_n$ at the intersection point of the n-th ellipse and the n-th hyperbola. An algorithm for transitioning from the top height $r_0$ to any of the following intersection heights of the nested layers is described below.

## 4.1 Arrays of $r_n$ Heights

Firstly, we apply to our optical construction two conditions that will optimize the neutron transport it can provide. These conditions will be used to transition between any two consecutive layers of the system.

To begin with, we want ray 1, reflecting off the edge of the upper layer in Figure 7, to reach the other edge of the layer, so that it does not get lost by the system. Second, we also require that the ray that gets reflected at $R_n$ by the

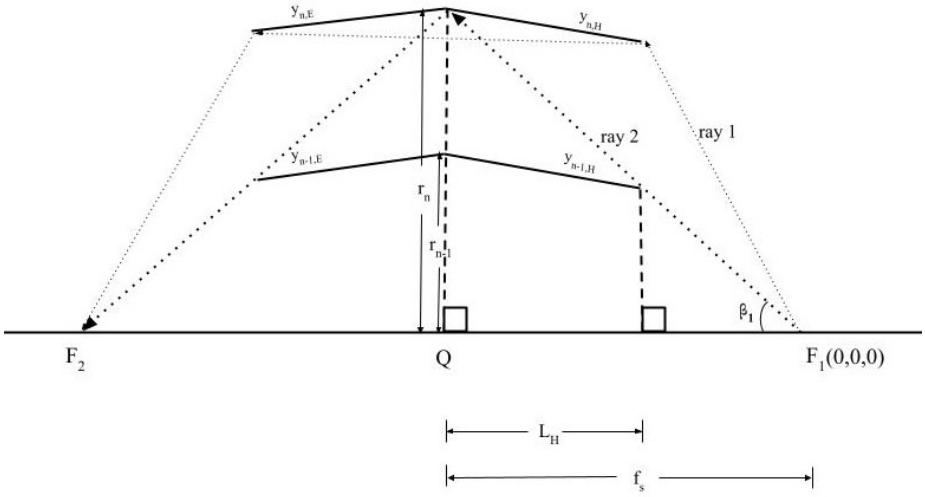


Figure 7: Conditions for Nesting Wolter Optics

upper layer (ray 2) would pass just over the surface of the nested hyperbola, so that all rays at higher glancing angles will get collected by the lower layer.

The first condition can be used to define an appropriate length $L_E$ of the ellipse for any given starting parameters of the system. The author of the document apologizes for not having the time to do that.

The second condition allows us to derive the following equation:

$$tan(\beta_n) = \frac{y_{n-1,H}(L_H - f_s)}{f_s - L_H} = \frac{r_n}{f_s} \tag{61}$$

$$y_{n-1,H}(L_H - f_s) = r_n \frac{(f_s - L_H)}{f_s} \tag{62}$$

Now, a little trick that was discovered empirically is applied. We assume (it will be proved later) that

$$\frac{y_{n-1,H}(L_H - f_s)}{y_{n,H}(L_H - f_s)} = \frac{r_{n-1}}{r_n} \tag{63}$$

So

$$y_{n-1,H}(L_H - f_s) = \frac{r_{n-1}}{r_n} y_{n,H}(L_H - f_s) \tag{64}$$

Substituting this back into equation 62:

$$\frac{r_{n-1}}{r_n} y_{n,H}(L_H - f_s) = r_n \frac{(f_s - L_H)}{f_s} \tag{65}$$

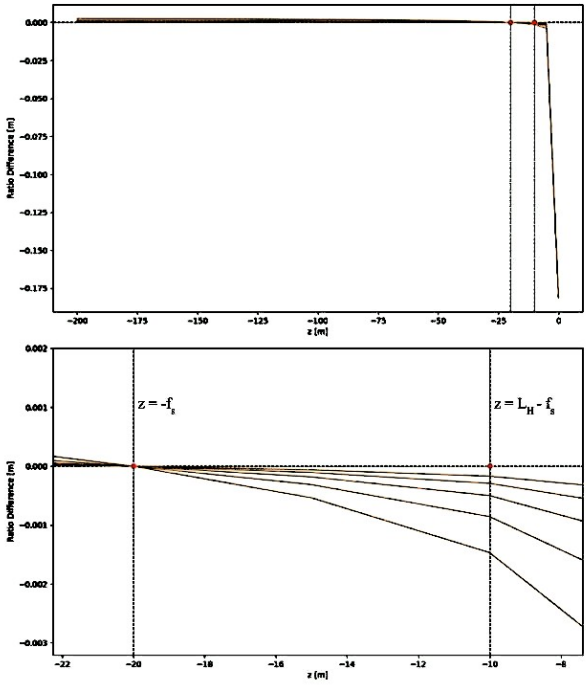


Figure 8: Differences between ratios $\frac{y_{n-1,H}(z)}{y_{n,H}(z)}$ and $\frac{r_{n-1}}{r_n}$ for different z-values of a system of six nested levels with a zoom-in into regions around $z = -f_s$ and $z = L_H - f_s$. The top line on the left corresponds to the difference for levels $n = 0$ and $n = 1$.

We arrive at an expression for $r_{n-1}$:

$$r_{n-1} = (r_n)^2 \frac{(f_s - L_H)}{f_s y_{n,H}(L_H - f_s)} \tag{66}$$

Now, this expression is used to test the assumption that it emerged from. On Figure 8, we plot

$$\frac{y_{n-1,H}(z)}{y_{n,H}(z)} - \frac{r_{n-1}}{r_n} \tag{67}$$

for z values covering the range from the start of the optics (z = 0) to the detector (z = -f). The y-values are calculated using the appropriate heights and equations 54-57 and 16.

The top plot shows that the approximation is very good for any coordinates z that come after the steep slope on the left part of the curve ($z < -5$ m). For such z, the difference between the two ratios is less than 0.004 at its extreme. The approximation works worst for the top layer, and improves as we go

deeper into the nested mirror arrangement. For the innermost layer ($n = 6$, $(n-1) = 5$) we get a maximum deviation of 0.0004 from a ratio difference of 0 in the region of $z < -5$ m. However, if we look at the lower plot, we can see that at the relevant z-coordinate z $= L_H - f_s$ the maximum difference for the two uppermost layers is 0.0014. This drops to 0.0002 for $n = 6$ ($(n-1) = 5$ curve). Rounding errors are negligible as the lower plot shows an almost perfect match of all layers at the intersection points $R_n$, where indeed, we would expect that $\frac{r_{n-1}}{r_n} = \frac{y_{n-1,H}(-f_s)}{y_{n,H}(-f_s)}$ as $y_{n-1,H}(-f_s) = r_{n-1}$ and $y_{n,H}(-f_s) = r_{n-1}$. Hence, the approximation holds for the purposes of the following simulations, and equation 66 can truly be assumed. (As an aside, a similar argument but for ellipses is provided in Appendix 2.)

Now that equation 66 was proven valid, it can be used recursively to define an array of intersection heights which can then be plugged back into equations 54-60 to calculate the parameters of each consecutive layer of optics.

### 4.2 Arrays of Semi-minor Axes ($b_{n,E}$ and $b_{n,H}$)

The semi-minor axes of the ellipses and the hyperbolas can be found from equations 54-60, 2 and 10, and an algorithm to do that is provided in the Jupyter notebooks. For engineering purposes, it is important to control that the spacing between consecutive layers does not get too small. The author of this narrative unfortunately did not have enough time to integrate this into the code, so it has to be checked manually.

## 5 Algorithm for Creating Wolter Optics for McStas

McStas provides the instrument component Guide anyshape, which allows us to import an OFF file with the dimensions of a specific guide, or an optical system. We consider three types of constructions that could be explored with nested Wolter optics: monoplanar, double planar and toroidal [12]. The monoplanar arrangement consists of optics in only two dimensions as shown on Figure 9 a). The double planar structure is made of two monoplanar optics rotated at right angles to each other (see Figure 9 b)). Finally, the toroidal arrangement consists of nested cylinders of optics (Figure 9 c)).

To construct these optics, an algorithm for creating OFF files is developed. The OFF file format starts with a line reporting the number of vertices, faces and edges (the last can be left as 0) that have to be constructed. After that the file gives the coordinates of each of the vertices in some set order, followed by lines connecting these coordinates into faces. In order to encode monoplanar optics in OFF files, we cut each mirror into rectangles and record them as the faces. Firstly, we go around the z-axis and split the range covered

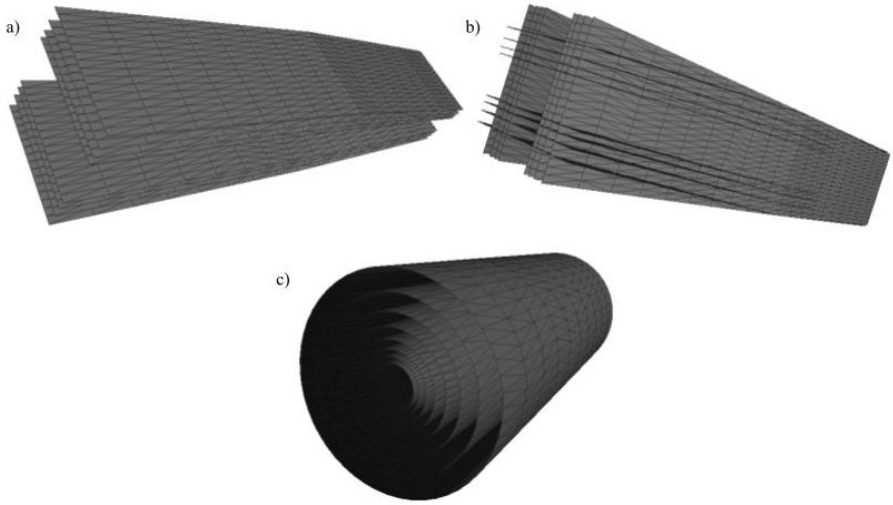


Figure 9: a) Monoplanar, b) Double planar, c) Toroidal (Hypothetical, not created)

by the optics into some input number of segments. Then, we calculate the intersection heights, $r_n$, for each nested level via equation 66. For each of these heights (so for each nested level), we go along the endpoints of the z-segments and derive their y-coordinates from equations 54-60. Both negative and the positive y-values are taken into account, as they represent the two mirrors below and above the optical axis. Finally, the x-axis could also be split into segments and for each of those, the x and y coordinates of each point along the z-axis could be calculated. It is also possible, and easier for simulations to handle, to skip this last step and consider each big panel along the entirety of the used x-coordinates as one face. Afterwards, this method is repeated for all of the other nested levels. The algorithm relies on setting a specific order of appearance of the coordinates in the OFF file, so that they can be more easily connected into faces by the appropriate code (as explained in Appendix III).

Once monoplanar optics are created, a second pair of them can be produced and rotated by 90 degrees so that it becomes perpendicular to the first. We call this a double planar arrangement. The same algorithm as before can be used to produce a second monoplanar optic but its x and y coordinates have to be exchanged in order to rotate it.

A toroidal optic is a proposed geometry in which the mirrors encircle the beam from all sides. A big advantage of this optic would be that it would only require one reflection by its hyperbolic section and one by the elliptical one to change both the x and the y components of a neutron's velocity. In

comparison, a double planar optic requires 4 such reflections - two from each plane of the optics. Since a toroidal optic could transport neutrons with less reflections, less neutrons will be lost during the interactions with the mirrors. The m value of the mirrors will determine the exact absorption rate but, as an example, if the probability of absorption is 20 percent, then a toroidal optic will transport 0.8 x 0.8 N = 0.64 N of N neutrons, and for a double planar one, the flux will reduce to 0.8 x 0.8 x 0.8 x 0.8 = 0.41 of the original one. Hence, toroidal optics may prove to be much more efficient then planar ones.

A disadvantage to the toroidal set-up would then be that it might be too hard to construct, as it will have to be made of many tiny elements, assembled into a continuum of hyperbolic and elliptical sections. It might therefore be useful to consider other regular polygons, such as hexagons or octagons of Wolter optics as a middle ground between planar and toroidal optics. For many of the incoming particles, such designs might be able to provide focusing with only two reflections, though some neutrons will still have to undergo the full 4 reflections.

# 6 Simulation Results

For the NNBAR experiment, there are two well-defined parameters - the maximum height $r_0 = 2$ m and the combined focal length, f, which is equivalent to the 200 meter length of the proposed beamline [5]. In addition, the set-up of the experiment is such that to prevent radiation leakage, two concrete blocks have been placed - a 'monolith' at 5.5 m, and a 'bunker' 15 m away from the source [5]. Whether any optics could be set in between would depend on the ability of their constituent materials to endure radiation and heat exposure. If the positioning of mirrors there would prove impossible, that would provide a lower limit to the distance between the source and the optics. If not, then the minimum distance would be the combined 5.5 meter length of the source and the large beam port (LBP).

Different set-ups within and outwith the boundaries of the monolith and bunker walls are tested here and some trends in the obtained FOM values are highlighted. Four parameters are varied in the system - the number of nested levels, n, the length of the hyperbolic section $L_H$ of the optics, the total length L, which defines the elliptical portion of the optics, and the distance from the source to the mirrors, $f_s$. Firstly, we will discuss one inherent property of the Wolter systems, and then we will see the effect of the number of nested mirrors on the figure of merit.

## 6.1 Position of Optics

It is important to remember that Wolter optics are only constructed for a specific position, as their hyperbolic sections have to begin at the z-coordinate

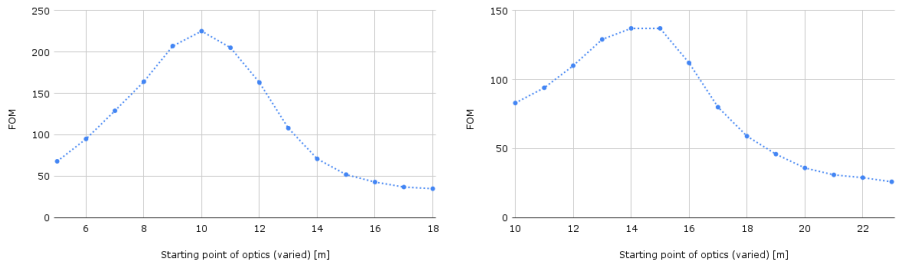


(a) $L = 40$ m, $L_H = 15$ m, $f_s = 25$ m, $n = 8$, starting point by design: 10 m

(b) $L = 40$ m, $L_H = 10$ m, $f_s = 25$ m, $n = 8$, starting point by design: 15 m

Figure 10: Variation in FOM value for two optics that are placed at different starting positions

$f_s - L_H$. To illustrate this point, two separate 8-layers optical systems are constructed, and their starting position is varied along the z-axis on Figure 10. For the first optics, $L = 40$ m, $L_H = 15$ m, $f_s = 25$ m. Hence, the optics is designed to be positioned at the z-coordinate $f_s - L_H = 25 - 15 = 10$ m. Indeed, if the OFF file of this optics is consulted, it will display 10 as its first z-coordinate. We can vary externally its position in the simulation by setting the optics at different coordinates in McStas. The results on Figure 10 a) show that the peak in FOM value is exactly at the designed starting point of the optic (10 m), which appears when the McStas component for the optics is set at z = 0. Deviating from this position leads to a decrease in the FOM, as the optics gets worse at focusing the neutron beam.

For the second simulation, the parameters $L = 40$ m, $L_H = 10$ m and $f_s = 25$ m are selected. Hence, the optics is designed to have its hyperbolic section starting at z = $f_s - L_H = 15$ m. Indeed, as before, we can see that the FOM values on Figure 10 b) peak around the starting point of 15 m, and there is a sharp decline in FOM as the optics position sways away from the optimum. Comparing the two simulations, it seems that optics with larger $L_H$ (Figure 10 a)), are better tuned to be placed further away from the source than their designated positions, while optics with smaller $L_H$ (Figure 10 b)) perform much worse even if their starting point is only slightly varied. We will see in further sections that the first mirror system has a ratio $\frac{L_H}{L}$ that is closer to $\frac{1}{3}$ than that of the second optic, so its $L_E$ length must be more appropriate to the chosen $L_H$ length. Hence, the first system is a closer approximation to the desired optimal Wolter optics of length L = 40 m, and is more efficient than the second one. In both cases however, it is important to remember that the starting position of the optic is integrated into its design, and the performance of the mirrors will only get worse if that is varied. For that reason, in all simulations that follow, the optics are placed only at their designated positions.

| | FOM | | | | | |
|---|---|---|---|---|---|---|
| n [levels] | case 0: L_H = 10, L = 50, f_s = 20, start of optics: 10 | case 1: L_H = 10, L = 40, f_s = 20, start of optics: 10 | case 2: L_H = 20, L = 40, f_s = 30, start of optics: 10 | case 3: L_H = 15, L = 30, f_s = 25, start of optics: 10 | case 4: L_H = 10, L = 20, f_s = 20, start of optics: 10 | case 5: L_H = 5, L = 10, f_s = 15, start of optics: 10 |
| 1 | 35 | 33 | 29 | 24 | 19 | 12 |
| 2 | 60 | 61 | 55 | 43 | 34 | 19 |
| 3 | 83 | 86 | 82 | 66 | 51 | 27 |
| 4 | 110 | 114 | 109 | 91 | 68 | 38 |
| 5 | 143 | 142 | 133 | 115 | 90 | 50 |
| 6 | 174 | 172 | 141 | 134 | 106 | 62 |
| 7 | 198 | 200 | 142 | 148 | 127 | 75 |
| 8 | 214 | 215 | 141 | 154 | 142 | 87 |
| 9 | 225 | 230 | 138 | 156 | 159 | 99 |
| 10 | 230 | 237 | 136 | 155 | 169 | 111 |
| 11 | 232 | 240 | 135 | 154 | 174 | 122 |
| 12 | 230 | 240 | 134 | 151 | 175 | 133 |
| 13 | 227 | 239 | 133 | 151 | 176 | 145 |
| 14 | | | | | | 155 |
| 15 | | | | | | 166 |
| 16 | | | | | | 175 |
| 17 | | | | | | 184 |
| 18 | | | | | | 190 |
| 19 | | | | | | 197 |
| 20 | | | | | | 202 |
| 21 | | | | | | 204 |

Figure 11: Raw data: FOM variation with different number n of nested mirrors for 4 Wolter optical systems

## 6.2 Varying n

In these simulations, the values of $L_H, L$ and $f_s$ were kept constant and only the number of layers in the system were varied. The simulation was run for four different optics with parameters described on Figure 12. All of the optics in this simulation are symmetric, having equal lengths $L_E$ and $L_H$ of their elliptical and hyperbolic sections. The raw data in Figure 11 show that all of the optics eventually reach a plateau in their FOM values, and after that adding more nested mirrors to the system does not drastically improve the figure of merit, or even slightly decreases it.

When the data from the symmetric optics on Figure 11 is plotted on Figure 12, the FOM plateau is not visible for the shortest optic, as it lies outwith the selected range of n values. The optics experience a shift in their FOM saturation point toward a larger value n of nested levels, as the total lengths L get shorter. It also appears that the longer optics can not produce a figure of merit that is equivalent to the ones given by the shorter optics. This might be because the increase in the length of the optics leads to a decrease in the time of flight after the reflection of the neutron. At some point the decrease in t outweighs the increase in the transported flux due to the larger acceptance of the longer mirrors. It is not necessary however that this optimal length is already reached at L = 10 m, as Figure 12 suggests. All optics that are plotted on that figure are symmetric, and therefore do not have $L_E$ controlled in such a way that the optimal ratio $\frac{L_E}{L_H}$ is reached. This ratio will be discussed more in section 6.4, but it is a possible explanation to the decrease in FOM that we

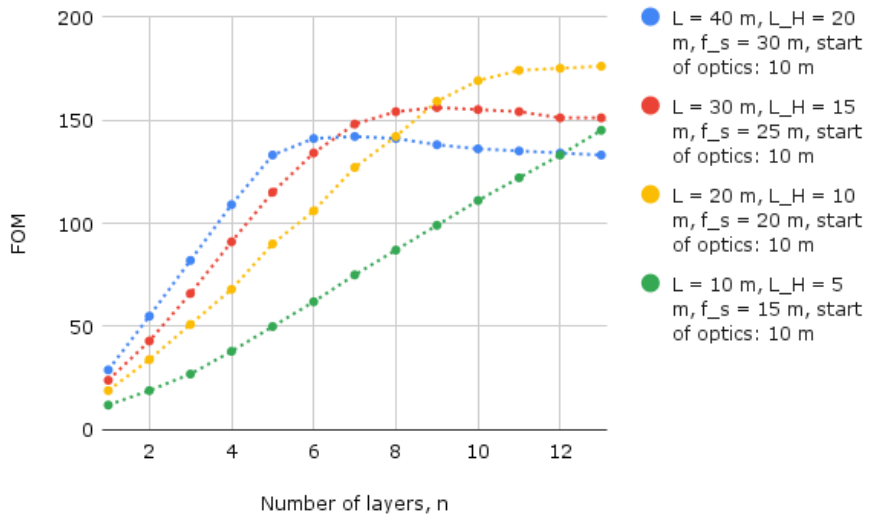


Figure 12: FOM variation with different number n of nested mirrors for 4 symmetric Wolter optical systems

observe as L gets larger.
A similar simulation was performed with asymmetric optics of $L_H = 10$ m, $f_s = 20$ m, and $L$ of 40 and 50 m. In contrast to Figure 12, the data on Figure 13 shows that there is no significant decrease in the maximum attainable FOM value as $L$ increases. It is therefore, complicated to predict the optimal length $L$ of the optics, but, as before, the plot shows a clear plateauing of the FOM value as some specific number n of nested mirrors is reached. This optimal n varies depending on the parameters of the system, and only for the simulations in this section, it already ranges from n = 6 to n = 21. Hence, it is important to check the exact value n for optimal FOM of each separate optical system that is simulated.

### 6.3 Varying $f_s$ and the starting position of the optics $(f_s - L_H)$

As discussed in Section 6.1, Wolter optics have a preassigned position of maximum FOM, so shifting their starting point is only possible by constructing anew an optic appropriate for that position. On Figure 14, the distance from the source to the intersection point $(f_s - L_H)$ is varied, and the optimal FOM for each separate optic is recorded for two different mirror arrangements. The plots show that for all optics there is a peak in FOM for mirrors designed to have a starting position at about 9 m. While for the longer 40 m optic this peak is flat and spreads out almost like a plateau, the shorter 30 m optic has a

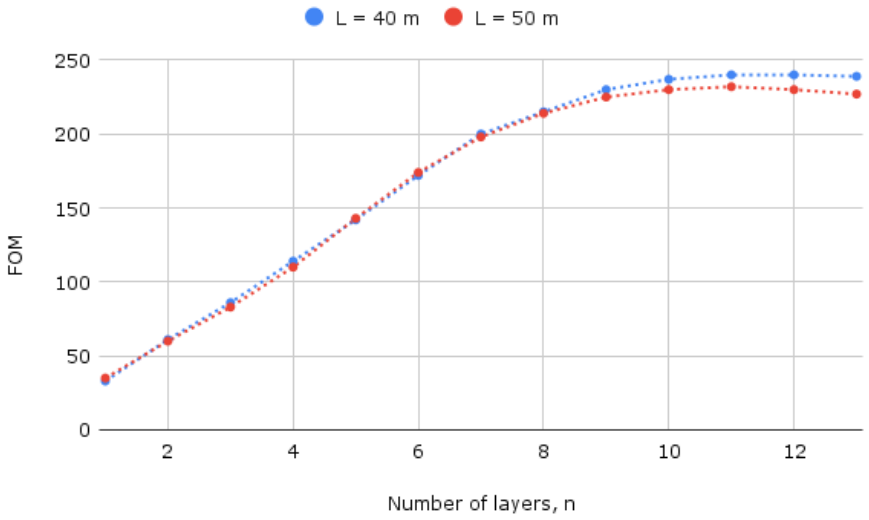


Figure 13: FOM variation with different number n of nested mirrors for 2 asymmetric Wolter optical systems ($L_H = 10$ m, $f_s = 20$ m)

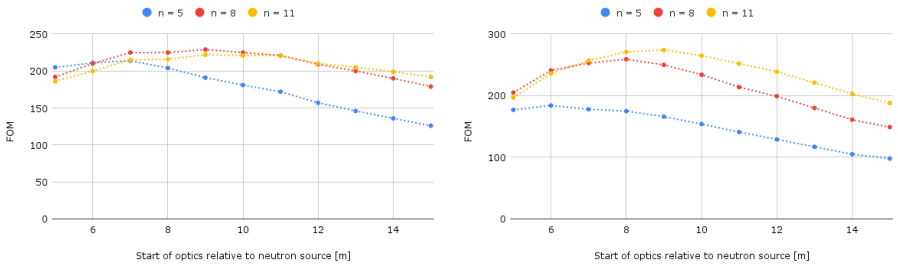


(a) $L = 40$ m, $L_H = 15$ m (b) $L = 30$ m, $L_H = 10$ m

Figure 14: Variation in FOM value as the optics is designed to be positioned further away from the source

more pronounced apex that encompasses a narrower range of mirror parameters. Hence, when longer mirrors are constructed, there is a greater allowance for selecting a starting position that returns a large FOM, but is positioned more than 9 meters away from the source. In addition, adding more nested levels to the system also shifts the peak of the figure of merit to a greater distance away from the source. This is important, because the NNBAR will probably require the optics to start somewhere after the bunker, which is positioned at about 15 m from the source, far from the 9 m FOM peak.

Figure 14 a) shows that for a 40 meter optic with $L_H = 15$ m, an 11-layered system would not produce a larger FOM than a stack of only 8 mirrors. This suggests that the excess material needed for constructing a larger optic might be compensated by the smaller number of nested mirrors that the optics would require. However, Figure 14 b) shows that shorter optics might outperform longer ones, as the overall FOM for the 30 m optic is larger than that for the 40 m optic. This is similar to the results obtained in the last section: even though longer optics will accept more neutrons, they also provide a smaller time of flight of the neutrons, because they reflect some of the neutrons closer to the detector. At some point this reduction of the time of flight decreases the figure of merit more than the increase in flux contributes to it. The exact length $L$ at which the optic becomes less efficient would be influenced by the ratio of $L_H$ to $L_E$, as discussed in the following section.

## 6.4 Varying $L_H$ and $L$

First the hyperbolic length $L_H$, and then the total length $L$ of the optics is varied, so that the ratio of $L_H$ to $L_E$ changes. Simulations are run for three set-ups with a different number of nested levels: n = 5, n = 8 and n = 11. The length $f_s$ is also varied in the first simulation, so that the starting point of the optics ($f_s - L_H$) is always set to 10 m. The total length $L$ is selected to be 40 m in this trial.

In the second simulation, $f_s$ is chosen to be 20 m, and the optics have $L_H =$ 10 m, so they again require to be placed at 10 m away from the source. The raw data from these simulations is provided in Tables 1.1 and 1.2, and plots of it are presented on Figures 16 and 17.

For both simulations, there is a peak of the FOM values at a certain ratio of $\frac{L_H}{L_E}$. For all scenarios that are simulated, this peak occurs roughly when $\frac{L_H}{L} = \frac{1}{3}$. Hence, we have

$$\frac{L_H}{L} = \frac{L_H}{L_H + L_E} = \frac{1}{3} \tag{68}$$

So,

$$3L_H = L_H + L_E \tag{69}$$

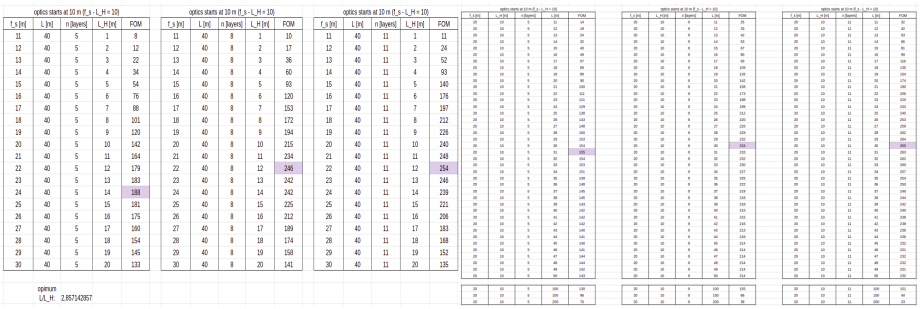

(a) Table 1.1: FOM values as a function of $L_H$ for different number of nested mirrors

(b) Table 1.2: FOM values as a function of $L$ for different number of nested mirrors

and

$$L_E = 2L_H \tag{70}$$

This is not a strict formula - even for the few set-ups that are simulated, the ratio of $L_H$ to L varies from 2.8 to 3.1, and is not equal exactly to 3. However, equation 70 is still a very good approximation for the scenarios that were investigated.

If the value of $L_H$ is known, then Figure 17 shows that overshooting a bit the value of $L$ that returns an optimum FOM does not lead to a very significant decrease in the figure of merit. In fact, after the maximum FOM is reached, values start to decline very gradually even as $L$ increases. On the opposite side of the curve, however, when the maximum FOM is still not achieved, adding longer elliptical sections (increasing $L$) has more influence on the figure of merit. It is therefore, a much better strategy to overshoot for $L_E$ (and $L$), then to undershoot for it.

If, however, we decide to settle on a value for $L$, instead of inputting one for $L_H$, the FOM values rise much more steeply as the correct $\frac{L_H}{L_E}$ ratio is approached (see Figure 16). It is therefore harder and less efficient to approximate the hyperbolic lengths to ones that would produce an optimal FOM. Inputting $L_H$, and striving to find the best $L$ value for it, is a better alternative to inputting $L$ and searching for the optimal $L_H$.

The first simulation also displays a shift of the optimal FOM values toward positions of smaller $L_H$ as more nested levels are added. This is reminiscent of the observations made in section 6.2, where symmetric optics of shorter length L would need more nested levels to reach their optimal figure of merit. In both cases, as the total length $L$ of the optics ($L = L_H + L_E$) decreases, more nested mirrors have to be added to reach the saturation of FOM that was observed on Figure 12.

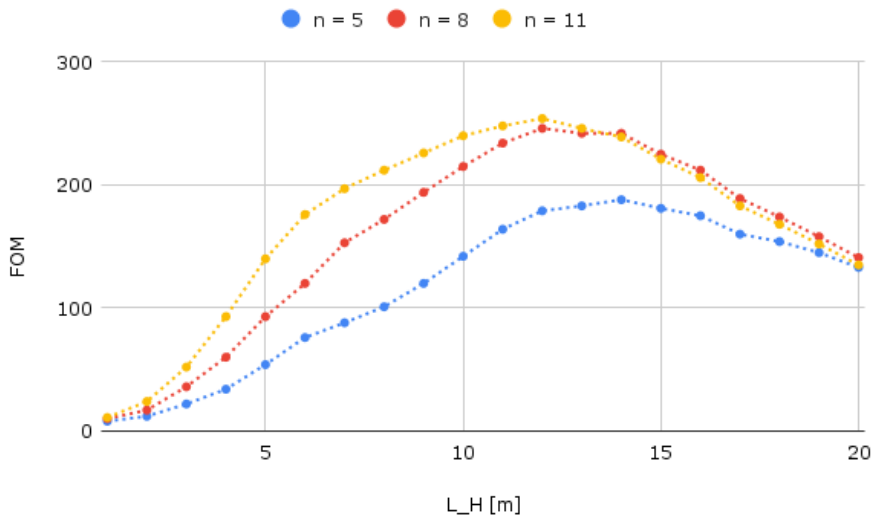


Figure 16: FOM values as a function of $L_H$ for different number of nested mirrors

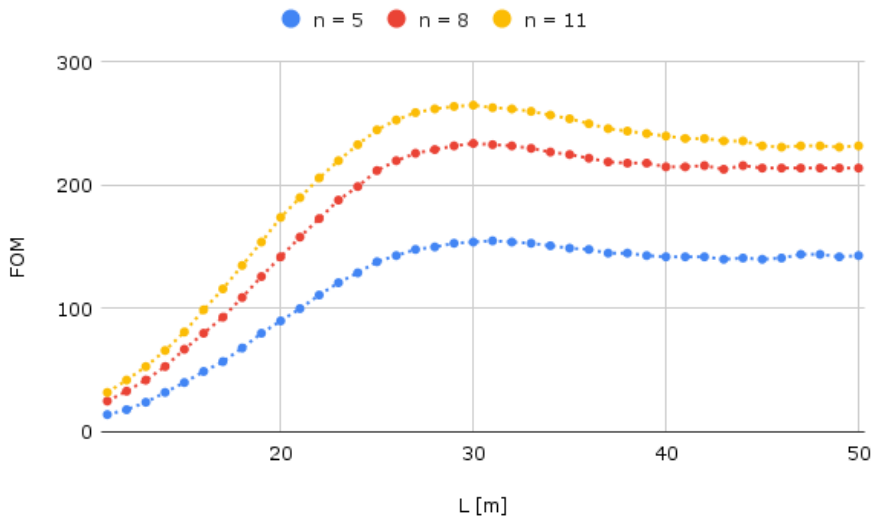


Figure 17: FOM values as a function of $L$ for different number of nested mirrors

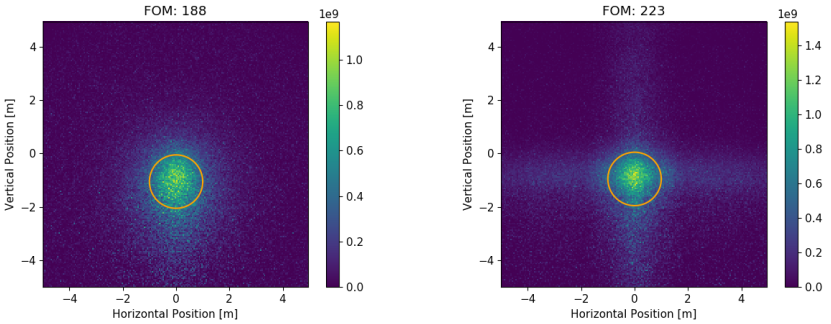


(a) FOM for a 40 m elliptical guide (b) FOM for a 40 m Wolter optic of $n = 11$

Figure 18: FOM comparison of an elliptical guide and a Wolter optic

Additionally, for both simulations in this section, the FOM value increases as more nested levels are added. The difference in FOM value between 5 and 8 nested levels is larger than that between 8 and 11 levels, which can be expected, as the optics must be approaching its FOM plateau by that point.

### 6.5 Comparison with an Elliptical Guide

To make a comparison between the efficacy of guides and Wolter nested optics for the NNBAR experiment, we construct a guide of length 40 m and place it at z = 10 m. From the previous sections, it can be estimated that an optic of a comparable length $L = 40$ m will perform best when $\frac{L_H}{L} = \frac{1}{3} = \frac{10}{30}$. In fact, the exact ratio of optimal FOM is given by Table 1.1, which provides results for $L = 40$ m optics. Hence, we know that the optimal FOM for a 40 m optic with 11 nested levels that is set at z = 10 m will be achieved when $L_H = 12$ m. This FOM is over 220, as signified by Table 1.1 and Figure 18, while the elliptical guide only produces a FOM of 188. Hence, it is possible to construct Wolter optics that are more suitable to the purposes of the NNBAR experiment than elliptical guides.

## 7 Conclusion

Even though Wolter optics could produce better results for the NNBAR experiment than elliptical guides, they still rarely achieve the figures of merit that are required. A FOM of 300 was not reached even once for the optics that were simulated, and the best FOM achieved was 274, when $L = 30$ m, $L_H = 10$ m, $f_s = 19$ m and z-start = 9 m (see Figure 14 b)). It is probably possible to construct an optic that returns an FOM of 300 or maybe even the desired 333, but the author is sceptical about whether a higher figure of merit could be reached with Wolter optics.

Therefore, Wolter optics might provide a solution to the NNBAR neutron transport problem, but it is also important to investigate other options for that experiment. For instance, it is possible that purely elliptical optics, such as the ones suggested by Oliver Zimmer [10], provide better figures of merit than Wolter optics. If only elliptical mirrors are used, this will reduce the absorption rate by the reflector, since only two reflections will be required to direct the beam, as opposed to the four reflections by a double planar Wolter optic. This increase in flux will however come at the expense of less focusing, as the ellipses will produce a more blurred image than Wolter optics. It is important, therefore, to simulate elliptical mirrors with the exact parameters of the NNBAR system, so that the better optic can be chosen.

Even if nested Wolter optics do not get used at the NNBAR experiment, they are still very promising for neutron transport. The FOM plots on Figure 18 show that Wolter optics have a better focusing ability than the conventional guides. Hence, they can be useful in neutron transport to small samples or where precision in the width of the transported beam is required. In addition, when the time of flight reset was turned off by accident in the FOM calculations, the simulations achieved stunning FOM values that could reach more than 800. This suggests that the Wolter optics are really good at transporting a large number N of neutrons, so they can be useful in experiments that require an in-beam transport of a large flux.

# References


[1] Pareschi G, Spiga D, Pelliciari C. X-ray Telescopes Based on Wolter-I Optics. In: The WSPC Handbook of Astronomical Instrumentation: Volume 4: X-Ray Astronomical Instrumentation. World Scientific; 2021. p. 3-31.

[2] VanSpeybroeck L, Chase R. Design parameters of paraboloid-hyperboloid telescopes for X-ray astronomy. Applied Optics. 1972;11(2):440-5.

[3] Thompson PL, Harvey JE. Aplanatic Wolter Type-I telescope design: is there a practical advantage? In: X-Ray Optics, Instruments, and Missions. vol. 3444. SPIE; 1998. p. 526-42.

[4] Hussey DS, Abir M, Cook JC, Jacobson DL, LaManna J, Kilaru K, et al. Design of a neutron microscope based on Wolter mirrors. Nuclear Instruments and Methods in Physics Research Section A: Accelerators, Spectrometers, Detectors and Associated Equipment. 2021;987:164813.

[5] Addazi A, Anderson K, Ansell S, Babu K, Barrow J, Baxter D, et al. New high-sensitivity searches for neutrons converting into antineutrons and/or sterile neutrons at the HIBEAM/NNBAR experiment at the European Spallation Source. Journal of Physics G: Nuclear and Particle Physics. 2021;48(7):070501.

[6] Santoro V, Andersen KH, DiJulio D, Klinkby EB, Miller T, Milstead D, et al. Development of high intensity neutron source at the European Spallation Source. Journal of Neutron Research. 2020;22(2-3):209-19.

[7] Baldo-Ceolin M, Benetti P, Bitter T, Bobisut F, Calligarich E, Dolfini R, et al. A new experimental limit on neutron-antineutron oscillations. Zeitschrift für Physik C Particles and Fields. 1994;63(3):409-16.

[8] Frost M. Observation of Baryon Number Violation via Cold Neutron Sources. 2019.

[9] Khaykovich B, Gubarev M, Bagdasarova Y, Ramsey B, Moncton D. From x-ray telescopes to neutron scattering: Using axisymmetric mirrors to focus a neutron beam. Nuclear Instruments and Methods in Physics Research Section A: Accelerators, Spectrometers, Detectors and Associated Equipment. 2011;631(1):98-104.

[10] Zimmer O. Multi-mirror imaging optics for low-loss transport of divergent neutron beams and tailored wavelength spectra. arXiv preprint arXiv:161107353. 2016.

[11] Bagdasarova YS. Wolter mirror microscope: Novel neutron focussing and imaging optic. Massachusetts Institute of Technology; 2010.

[12] Howells MR. Mirrors for synchrotron-radiation beamlines. In: New Directions in Research with Third-Generation Soft X-Ray Synchrotron Radiation Sources. Springer; 1994. p. 359-85.

[13] Berendonk S. Proving the reflective property of an ellipse. Mathematics Magazine. 2014;87(4):276-9.

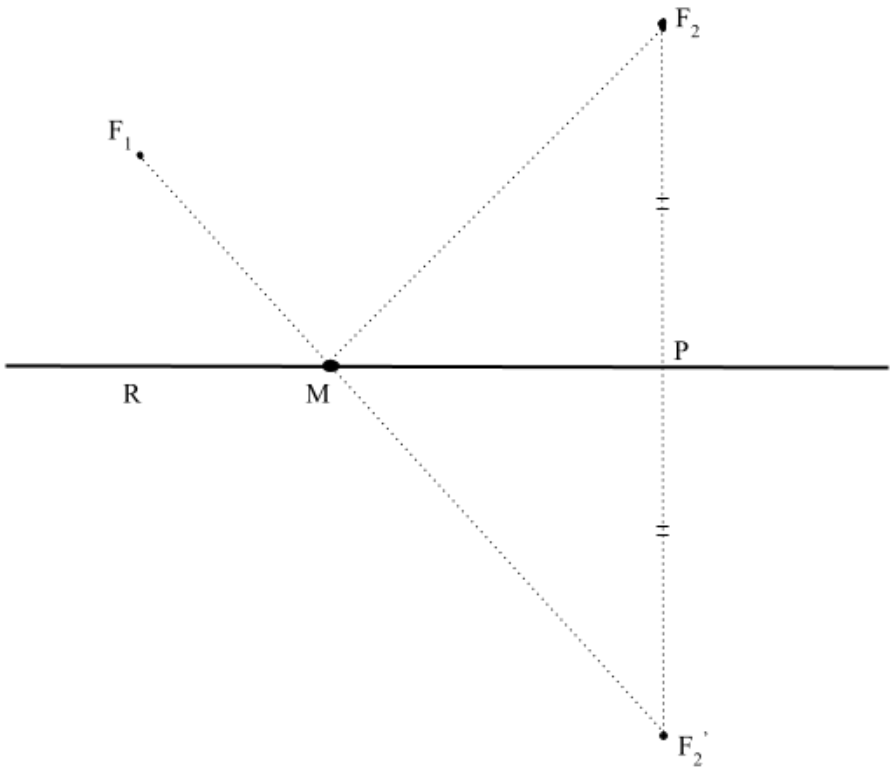


Figure 19: Proof of Reflection Property of Ellipse

# 8 Appendix I: Reflection by Conic Sections

## 8.1 Ellipse

It was stated in section 3.3.1 that a ray passing through one of the focal points of an ellipse and reflecting off its surface will head toward the other focus. We will prove this in two steps (also see [13]).

1) Firstly, consider two points and a line as on Figure 19. We want to find the shortest distance from the point $F_1$ to the point $F_2$ that touches the line. To do this, we reflect the point $F_2$ about the line to $F_2'$. Assuming that the shortest distance passes through some point M on the line, we notice that $\angle F_2MP = \angle F_2'MP$ and $F_2M = F_2'M$. Hence, $F_1M + MF_2 = F_1M + MF_2'$, so finding the shortest distance between $F_1$ and $F_2$ that touches the line is equivalent to finding the shortest distance from point $F_1$ to point $F_2'$. But we know that the shortest distance between two points is just the straight line connecting them. Therefore, point M must lie on the line $F_1F_2'$, so $\angle F_1MR = \angle F_2'MP = \angle F_2MP$. Hence, the shortest distance between two points that

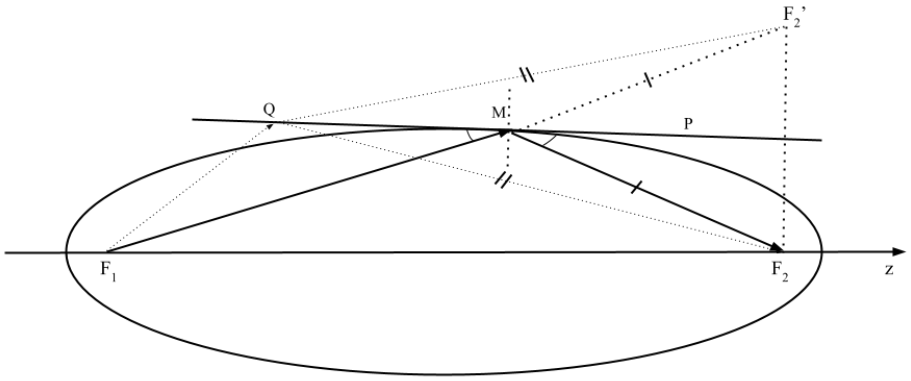


Figure 20: Proof of Reflection Property of Ellipse

passes through a given line is actually a reflection off the surface of the line.

2) We now use what we found in 1) to prove that if $F_1$ and $F_2$ are the two foci of an ellipse, then point M would lie on its surface. Firstly, we draw on Figure 20 an ellipse with its two foci and choose an arbitrary point M on its surface. We extend $F_1M$ by $MF_2'$ such that $MF_2' = MF_2$. We now draw a line l through M that bisects the line $F_2F_2'$. Hence $F_2'$ is a reflection of $F_2$ about the line l. We will show that this line has to be the tangent to the ellipse at point M.

We assume toward a contradiction that l is not tangent to the ellipse at point M. Hence, l has to touch the ellipse a second time. We call the point of intersection Q. Now we use the defining property of an ellipse - that it is the locus of points for which the sum of the distances to its two foci is constant. Hence, we have that $F_1Q + QF_2 = F_1M + MF_2 = F_1M + MF_2' = F_1F_2'$. But from triangle $F_1QF_2'$ we know that this can not be true - the sum of two of sides of a triangle always has to be greater than the length of the other side. Hence, we have arrived at a contradiction, and l must be the tangent line to the ellipse. Therefore, using 1), we know that the angles $\angle F_1MQ = \angle F_2MP$ are the glancing angles of incidence and reflection at point M on the surface of the ellipse, so indeed the ray $\overrightarrow{MF_2}$ is a reflection of the ray $\overrightarrow{F_1M}$. Since M was an arbitrary point on the ellipse, it is true that more generally any ray incoming from one of the foci of an ellipse reflects off its surface towards the other focus.

## 8.2 Hyperbola

A hyperbola has a very similar property - the reflection of a ray coming from one of its foci appears to be originating at its other focus. To prove this, we first draw an arbitrary ray starting at $F_1$ on Figure 21 that intersects the

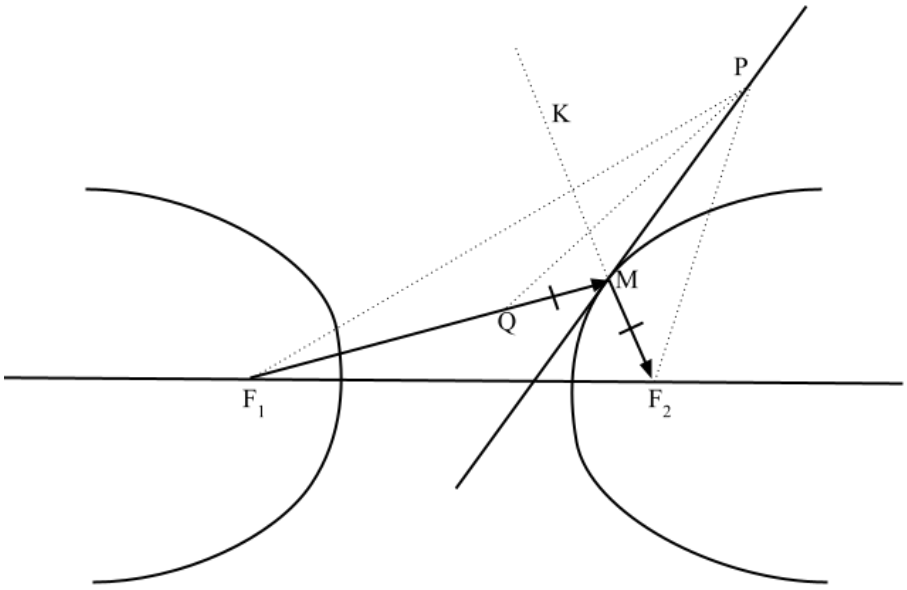


Figure 21: Proof of Reflection Property of Ellipse

hyperbola at point M. Then, we choose a point Q on $F_1M$ such that $QM = MF_2$. We can see that $F_1Q = F_1M$ - $QM = F_1M$ - $MF_2$. This is important because a hyperbola is defined as the locus of points for which the difference of the distances to the two foci is constant. We now know that this constant is equal to $F_1Q$.

Now we call L the midpoint of $MF_2$. Triangles $LMQ$ and $F_2ML$ are equivalent, so the angles $\angle LMQ$ and $\angle LMF_2$ are equal. Similar to the ellipse case, we now only need to prove that LM lies on the tangent to the hyperbola at point M to conclude that the reflective property is satisfied. To do this, we once again assume towards a contradiction the contrary.

If LM is not lying on a tangent line to the ellipse, then it must intersect it one more time. We call this second point of intersection P. Noticing that QP = $PF_2$, we have $F_1Q + QP > PF_1$, so $F_1Q > PF_1 - PF_2$. But this means that $PF_1 - PF_2 \neq F_1Q$, so the point P can not lie on the hyperbola. Thus, we have a contradiction, and the line MP must be part of the tangent to the ellipse at point M. If we extend that tangent as on Figure 21, we get that $\angle LMF_2 = \angle PMK$ (P not on the surface of the hyperbola, as proven). But we have already found that $\angle LMQ = \angle LMF_2$, so we have that $\angle LMQ = \angle PMK$. Hence $\overrightarrow{MK}$ is a reflection of ray $\overrightarrow{F_1M}$. But MK is an extension of the line $F_2M$, so indeed it appears that the reflection of $\overrightarrow{F_1M}$ coming from the first focal point of the hyperbola originates from the other focus ($F_2$). Because M

was an arbitrary point, we can generalise this property to all points on the surface of the hyperbola.

# 9 Appendix II: Ellipse Approximation

In section 3.1 an approximation was made to establish the arrays of heights at the intersection point. It argued that for the bulk of the hyperbola surface, the ratios between the heights of two consecutive hyperbola layers are preserved at any point on the z-axis. A similar argument applies for an ellipse.

On Figure 22,

$$\frac{y_{n-1,E}(z)}{y_{n,E}(z)} - \frac{r_{n-1}}{r_n} \tag{71}$$

is plotted for the range of z values covering the surface of the ellipses.

For z-values to the left of the intersection point ($z < -f_s$), the maximum value of the ratio difference is 0.0015, so $\frac{r_{n-1,E}}{r_{n,E}}$ can be approximated to $\frac{y_{n-1,E}(z)}{y_{n,E}(z)}$ for the coordinates that define the ellipse portion of the Wolter set-up. As with the hyperbolas, the approximation becomes better going inwards into the nested mirror system. In addition, the mid-sections of the different ellipses are also covered by this slice of the z-axis, so it might be relevant for the construction of nested elliptical optics.

# 10 Appendix III: Python Code and How Navigate through the Jupyter Notebooks

## 10.1 General Functions

There are eight basic functions for creating the Wolter Optics parameters that might appear in a number of different notebooks.

Equations 31, 35 and 37 are summarised by the functions theta(), c_of_hyperbola() and c_of_ellipse().

```
import numpy as np

#Helper functions

def theta(r_i,f_i,f_s):

    θ = (np.arctan(r_i/f_i) + np.arctan(r_i/f_s))/4
    return
```

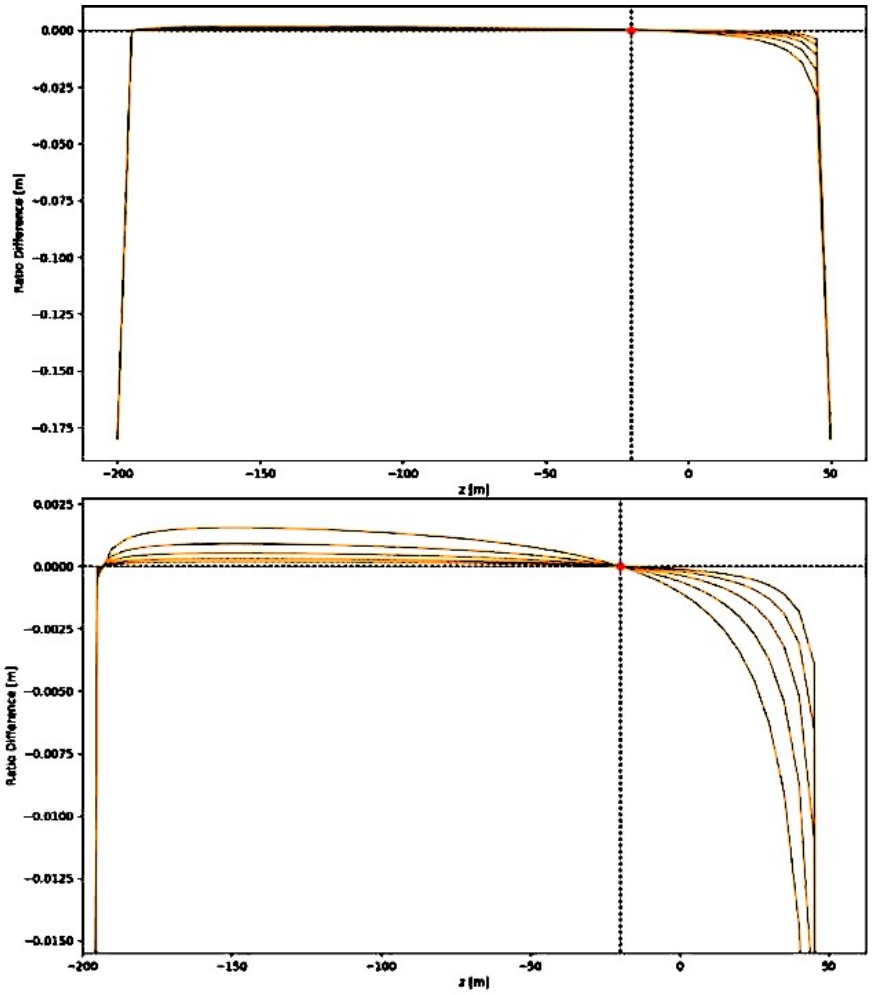


Figure 22: Differences between ratios $\frac{y_{n-1,E}(z)}{y_{n,E}(z)}$ and $\frac{r_{n-1}}{r_n}$ for different z-values of a system of six nested levels with a zoom-in into the region $2c_0, H > z > -f$. The top line on the left corresponds to the difference for levels $n = 0$ and $n = 1$.

```
def c_of_hyperbola(r_i,f_i,f_s):

    θ = theta(r_i,f_i,f_s)
    c_H = 0.5*(r_i/(np.tan(np.arctan(r_i/f_s) - 2*float())) - f_s)
    return c_H

def c_of_ellipse(r_i,f_i,f_s):

    θ = theta(r_i,f_i,f_s)
    c_H = c_of_hyperbola(r_i,f_i,f_s)
    c_E = (f_s + f_i)/2 + c_H
    return c_E
```

The semi-minor half axis of an ellipse is defined by equations 60 and 8, the three functions above, and the ellipse_half_axis() function. The function hyperbola_half_axis uses equations 44 and 53 to define the semi-minor axis of a hyperbola.

```
#Ellipse semi-minor axis at height r_n
def ellipse_half_axis(r_n, f_i, f_s):

    c_n_H = c_of_hyperbola(r_n, f_i, f_s)
    c_n_E = c_of_ellipse(r_n, f_i, f_s)

    L = f_s - c_n_E + 2*c_n_H

    t = ((L**2 + c_n_E**2 + r_n**2) + np.sqrt((L**2 + c_n_E**2 + r_n**2)**2
    - 4*(c_n_E**2)*(L**2)))/2

    if t >= 0:
        a_n_E = np.sqrt(t)
        b_n_E = np.sqrt(a_n_E**2 - c_n_E**2)
    else:
        print('Warning: Negative value under square root')

    return b_n_E

#Hyperbola semi-minor axis at height r_n
def hyperbola_half_axis(r_n, f_i, f_s):

    c_n_H = c_of_hyperbola(r_n, f_i, f_s)

    N = c_n_H**2 + (f_s + c_n_H)**2 + r_n**2
    g = (N - np.sqrt(N**2 - 4*(c_n_H**2)*((f_s + c_n_H)**2)))/2

    if g >= 0:
```

```
        a_n_H = np.sqrt(g)
        b_n_H = np.sqrt(c_n_H**2 - a_n_H**2)
    else:
        a_n_H = 0
        b_n_H = 0
        print('Warning: Negative value under square root')

    return b_n_H
```

Then equations 60 and 57 are encoded by the functions ellipse() and hyperbola() which give y-coordinates for different values along the z-axis.

```
def ellipse(r_n, f_i, f_s, z):

    c_n_H = c_of_hyperbola(r_n, f_i, f_s)
    c_n_E = c_of_ellipse(r_n, f_i, f_s)
    b_n_E = ellipse_half_axis(r_n, f_i, f_s)

    L = f_s - c_n_E + 2*c_n_H
    t = ((L**2 + c_n_E**2 + r_n**2) + np.sqrt((L**2 + c_n_E**2 + r_n**2)**2
    - 4*(c_n_E**2)*(L**2)))/2

    if t >= 0:
        a_n_E = np.sqrt(t)
    else:
        print('Warning: Negative value under square root')
    y_n_E = b_n_E*(np.sqrt(1 - ((z + c_n_E - 2*c_n_H)**2)/(a_n_E**2)))

    return y_n_E

def hyperbola(r_n, f_i, f_s, z):

    c_n_H = c_of_hyperbola(r_n, f_i, f_s)
    N = c_n_H**2 + (f_s + c_n_H)**2 + r_n**2
    g = (N - np.sqrt(N**2 - 4*(c_n_H**2)*((f_s + c_n_H)**2)))/2

    if g >= 0:
        a_n_H = np.sqrt(g)
        b_n_H = np.sqrt(c_n_H**2 - a_n_H**2)
    else:
        a_n_H = 0
        b_n_H = 0
        print('Warning: Negative value under square root')

    y_n_H = b_n_H*(np.sqrt(((z - c_n_H)**2)/(c_n_H**2 - b_n_H**2) - 1))
    return y_n_H
```

Finally, an array of $r_n$ heights is generated from the height of the top intersection point ($r_0$) by using equation 67.

```
def heights(r_0, f_i, f_s, n):
    h = [r_0]
    r = r_0
    for i in range(1,n):
        q = hyperbola(r, f_i, f_s, z = L_H - f_s)
        r = (r**2)*(f_s - L_H)/(q*f_s)
        h.append(r)
    return h
```

## 10.2 final_half_axes()

This notebook can be used to create arrays of semi-minor ellipse and hyperbola axes from given $r_0, f_i, f_s, L_H, L$ and n. The notebook also visualises the system (via the function wolter_plot) and creates the plots which test the assumption that led to equation 69 and the appropriate intersection heights for nesting the mirrors.

## 10.3 mono_planar_off_file_creation

This notebook creates OFF files for horizontal monoplanar nested systems. The optics will have to be rotated externally after being imported into McStas to get a vertical arrangement.

The coordintes() function assigns appropriate y-values to each z coordinate and splits the x-axis into an arbitrary number of segments. These coordinates are then written down in the off file by the function monoplanarOFF. The coordinates are first ordered according to the nested level they belong to. For each nested level, first the coordinates of the upper mirror are encoded, then those of the lower mirror. For each mirror, coordinates are ordered starting from the front right corner of the optics and going along the z-axis for each fixed x coordinate. The code ensures that the coordinates of the last x-value and those at the end of each line z-positions are not used to begin writing a new face, as there would be no coordinates following them that could be used to finish the face.

## 10.4 double_planar_off_file_creation and simplified_double_planar

The double planar arrangement consists of two monoplanar systems at right angles to each other. The monoplanar optics are created in the same manner as before, but the doubleplanarOFF() function exchanges the x and y coordinates of one of them, so that it gets rotated.

The double_planar_off_file_creation notebook produces a file with more faces, as it also splits the optics along the x-axis (x = -2, x = -1.75, x = 1.5, etc). This is why this notebook is heavier than simplified_double_planar where only the z and y axes are segmented and panels go along the whole x dimension (x = -2 to x = 2 for NNBAR). The extra panels should not make much difference to the results, so it is recommended to use the simplified version to get faster simulations.

## 10.5 NNBAR_TestEnvironment_Wolter

This notebook was created by Richard Wagner. It can be used to test a single OFF file as an optics arrangement for the NNBAR experiment. The mirrors should be set at (0, -0.273, 0) in the code, so that they start at the correct position for the Wolter optics. The y-coordinate is set to -0.273 to account for the specifications of the source - there is more neutron flux below the optical axis than above it.

## 10.6 fast_NNBAR

This notebook is almost identical to the previous one, but it allows you to test an OFF file by placing the optics sequentially at multiple coordinates. As was found (and expected from theory), the Wolter optics has only one proper coordinate, as it is designed for a specific distance from source to the optics ($f_s - L_H$). Hence, the reflector has to be set at z = 0, as previously suggested, since the OFF file already contains the appropriate start point of the optics. It can checked artificially by opening the OFF file and examining the first z-coordinate that is present there or it can be calculated as $f_s - L_H$. Unless one wants to replicate the results from tables 1 and 2, and verify that Wolter optics focus well only when they are positioned correctly, one would not find much use in this notebook.